Available online at www.sciencedirect.com
SCIENCE DIRECT
Chemical Physics Letters 423 (2006) 344–351
CHEMICAL PHYSICS LETTERS
www.elsevier.com/locate/cplett

Terahertz vibration–rotation-tunneling (VRT) spectroscopy of the d_6-water trimer: Complete characterization of the 2.94 THz torsional band ($k^n = \pm 2^1 \leftarrow 0^0$)

Jia-xiang Han, Lynelle K. Takahashi, Wei Lin, Eddy Lee, Frank N. Keutsch [1], Richard J. Saykally *

Department of Chemistry, University of California, Berkeley, CA 94720-1460, United States

Received 13 January 2006; in final form 17 March 2006
Available online 4 April 2006

Abstract

We report the measurement and analysis of the complete perpendicular $k^n = \pm 2^1 \leftarrow 0^0$ $(D_2O)_3$ torsional band (origin 2940.9376(3) GHz), the upper state of which is the highest-energy (98.09912 cm^{-1}) torsional state yet observed. All known torsional transitions were included in a new global analysis of the six observed torsional bands, using the effective Hamiltonians derived by van der Avoird et al. [M. R. Viant, M. G. Brown, J. D. Cruzan, R. J. Saykally, M. Geleijns, A. van der Avoird, J. Chem. Phys. 110 (1999) 4369; A. van der Avoird, E. H. T. Olthof, P. E. S. Wormer, J. Chem. Phys. 105 (1996) 8034]. The experimental results will facilitate the descriptions of three-body interactions in water intermolecular potential energy surfaces (IPSs).

1. Introduction

The goals of current water cluster studies are to characterize the detailed nature of forces underlying the determination of a universal intermolecular potential energy surface (IPS) for general modeling of the properties of water, and to characterize the complex tunneling dynamics occurring in the aqueous hydrogen-bond network [1,2]. Even the best available theoretical ab initio IPSs cannot quantitatively reproduce experimentally determined properties of both liquid water and water clusters [2,3]. Recently, however, accurate and highly detailed empirical intermolecular potentials have been developed for water from the THz VRT spectroscopic data of water dimers [4–6], and have been shown to reproduce structures of clusters up to hexamer as well as the partial structural features of liquid water [7] and the detailed spectroscopic observables of the dimer. Previous studies have indicated that two-body and three-body interactions account for ca. 75% and 20% of the hydrogen binding energy, respectively, with all higher-body interactions contributing only ca. 5% of the binding energy [8,9]. Recent ab initio calculations of three-body interactions also indicate that three-body effects have significant influence on the barrier heights of the water trimer potential surface [10]. Detailed studies of water cluster trimers, $(H_2O)_3$ and $(D_2O)_3$, are therefore needed to refine the three-body interactions of the empirical water IPS.

Since the first spectra of the water trimer $(D_2O)_3$ were observed in 1992 [11], extensive experimental data have been compiled for both $(D_2O)_3$ and $(H_2O)_3$, as well as for related isotopomers. As shown in Fig. 1, six torsional bands of $(D_2O)_3$ [12–16] have been observed and two non-degenerate and three degenerate torsional vibration states have been characterized. Likewise, for $(H_2O)_3$ trimers (not shown), three torsional bands [12,17] have been observed and one non-degenerate and two degenerate torsional vibration states have been characterized. The torsional vibrations of mixed water trimer isotopomers [18,19] have

* Corresponding author. Fax: +1 510 642 8369.
E-mail address: saykally@berkeley.edu (R.J. Saykally).
[1] Present address: Department of Chemistry, University of Wisconsin-Madison, WI 53706, United States.

0009-2614/$ - see front matter © 2006 Elsevier B.V. All rights reserved.
doi:10.1016/j.cplett.2006.03.079

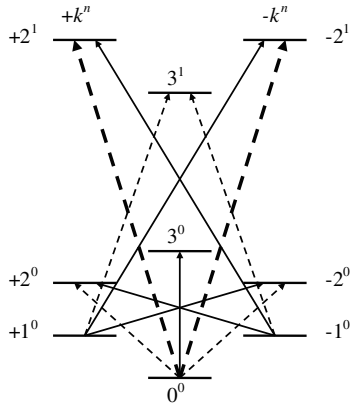

Fig. 1. Observed torsional energy levels for the observed $(D_2O)_3$ vibrations. The notation k^n $(=|k,n\rangle)$ is employed, with the quantum number $k = 0, \pm1, \pm2, 3$ and the index $n = 0, 1, 2, \ldots$. Dashed arrows indicate perpendicular transitions $(K' - K'' = \pm1)$ and solid arrows indicate parallel transitions $(K' - K'' = 0)$. The heavy dashed arrow corresponds to the present band $\pm2^1 \leftarrow 0^0$. A total of six torsional bands have been observed, and all 823 rotational transitions are included in the global fit.

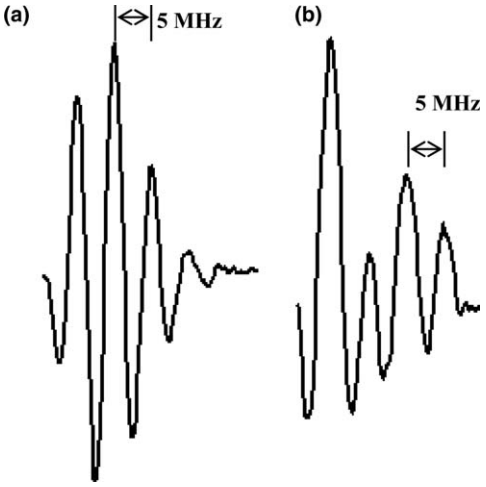

Fig. 3. A representative 5 MHz bifurcation tunneling quartet splitting from the $\pm2^1 \leftarrow 0^0$ torsional band. A splitting pattern (a) with nuclear spin weights of (76:108:54:11) is typical for all D_2O trimer transitions except for $K = 0 \leftarrow 1$. An irregular intensity pattern (b) is observed for $K = 0 \leftarrow 1$ transitions, with overall spin weights of (245:50:108:75).

also recently been studied with the Berkeley THz spectrometers as have a translational band of $(D_2O)_3$ and a librational band of $(H_2O)_3$ [20,21]. Details can be found in the review by Keutsch et al. [22].

As evident from the observed THz VRT spectra, the vibrationally averaged structure of the water trimer is a cyclic, chiral, quasiplanar ring structure, shown in Fig. 2. Due to the low barrier effective potential energy surface, flipping motion of the non-hydrogen-bonded hydrogen atom from one side of the three oxygen atom plane to the other side has a large amplitude. Superposition of the flipping motions generates a characteristic torsional energy level pattern, shown in Fig. 3.

Sixty-nine VRT transitions of the D_2O trimer located in the region from 2883 to 2962 GHz were first observed and analyzed by Liu et al. [12], and were refitted in the global analysis by Viant et al. [15]. In this Letter, we report the measurement and analysis of a complete torsional band having an origin of 2940.9376(3) GHz, which is the highest-energy torsional band observed so far. The spectra exhibit the characteristics of an oblate symmetric top (C_3) complying with perpendicular selection rules, and have been assigned as $k^n = \pm2^1 \leftarrow 0^0$. The bifurcation tunneling quartet splittings are evident in all observed transitions.

2. Brief theoretical background

2.1. Torsion tunneling

As shown in Fig. 2a, illustrating the torsional tunneling motion, one free hydrogen flips from a global equilibrium structure through a transition state and then to another

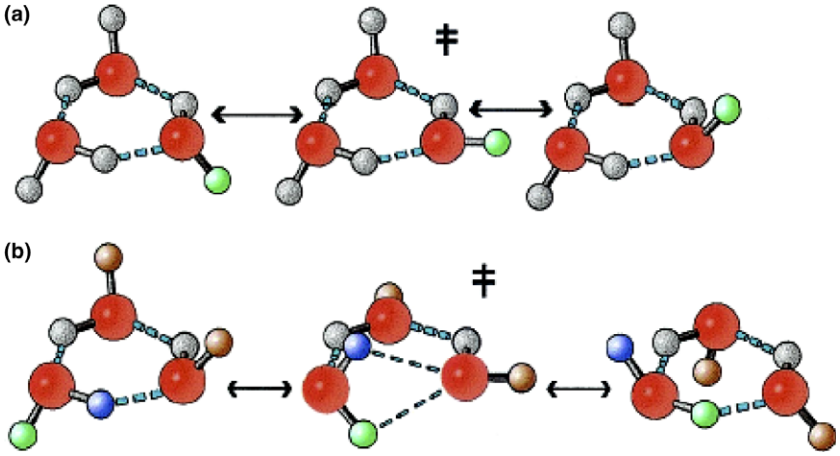

Fig. 2. Two distinct tunneling pathways rearrange the hydrogen bond network in the cyclic water trimer. The torsional (flipping) motion (a) of the free hydrogen atom from one side of the plane determined by three oxygen atoms to the opposing side connects six degenerate minima on the intermolecular potential energy surface (IPS). The bifurcation tunneling motion (b) in the water trimer consists of the exchange of a free hydrogen with a bonded hydrogen together with the flipping motion of the other free hydrogen atoms on the two neighboring water monomers.

equilibrium structure. The same torsional motion can occur for the other two free hydrogen atoms. The concerted flipping motion is symmetrically equivalent to rotation around the symmetry axis and thus is also called a 'pseudorotation', which couples strongly to the overall rotation of the trimer and results in a severe Coriolis perturbation. Ab initio calculations [23–25] indicate that six equilibrium structures, with two free hydrogen atoms at one side and one hydrogen atom at the opposing side of the oxygen plane, are connected by these torsional motions and that the corresponding barrier on the IPS is very low.

The torsional motion can be mathematically described by applying the permutation–inversion (PI) symmetry group [11–19,22,26]. The PI group associated with the torsional flipping between the six equivalent minima on the potential surface is the cyclic group G_6, which is isomorphic to the point group C_{3h}. The complex irreducible representations (irreps) of this group are conveniently labeled by the quantum number $k = 0, \pm 1, \pm 2, 3$ (modulo 6). Fig. 1 shows the diagram of the nine lowest torsional energy levels of $(D_2O)_3$, along with all of the currently observed vibrational transitions. The levels with $k = 0$ and 3 are non-degenerate, while those with $k = \pm 1$ and ± 2 are twofold degenerate. In the figure, a notation of k^n (equivalent to $|k, n\rangle$) with the index $n = 0$, or 1, ... is used to specify a torsional energy level. Transitions between these energy levels follow the selection rule [15,17,26]:

$$(k'' - K'') - (k' - K') = 3(\text{modulo } 6) \tag{1}$$

where K is the normal symmetric top projection quantum number, with the usual labeling (J, K). This rule allows the band characteristic (parallel or perpendicular) of a transition to be easily determined. For example, the transition $k^n = +2^1 \leftarrow 0^0$ is allowed with $(K' - K'') = -1$ and the transition $k^n = -2^1 \leftarrow 0^0$ is only allowed with $(K' - K'') = +1$; thus the $k^n = \pm 2^1 \leftarrow 0^0$ transitions are perpendicular bands.

2.2. Bifurcation tunneling

Bifurcation tunneling is the process that interchanges the free hydrogen with the bonded hydrogen in one water monomer of a trimer, in concert with the flipping motion of the free hydrogen atoms on the two adjacent water monomers. The pathway, which connects each of the six torsional minima with seven other inversions, is shown in Fig. 2b. The PI group G_{48} is employed to describe the bifurcation tunneling motion [22,26]. This motion actually has a very important role in determining the properties of liquid water, because it is the bifurcation tunneling that governs the breaking and reforming of the hydrogen bonds. The bifurcation tunneling will further split the torsional energy levels. Since the potential barrier for the bifurcation tunneling is much higher than that for the torsional tunneling, the bifurcation splittings are smaller than the torsional splittings. Details can be found in Refs. [26–29]. The effect of bifurcation tunneling in the observed water trimer spectra is seen in the quartet splitting patterns. Fig. 3a shows a typical observed trimer $(D_2O)_3$ absorption transition. The quartet splitting is a few MHz and varies a little in different bands for $(D_2O)_3$, while for $(H_2O)_3$, this quartet splitting is much larger – a few hundred MHz, as shown in Refs. [12,22]. In the present $(D_2O)_3$ torsional band, the splitting of the bifurcation tunneling is 5 MHz.

2.3. Effective rotational Hamiltonian

Detailed Hamiltonians have been derived for the water trimer [15,26]. The three water monomers are treated as rigid, with a ring structure. The non-rigid hydrogen bonds hold them together and the displacements occur only between the monomers. The total Hamiltonian H is expressed as:

$$H = H^{\text{rot}} + H^{\text{cor}} + H^{\text{int}} \tag{2}$$

where H^{rot} is simply the oblate symmetric rotor Hamiltonian for the overall rotation of the trimer. H^{cor} expresses the Coriolis coupling between the overall angular momentum and the internal angular momentum generated by the torsional motions of three monomers. The last term, H^{int}, describes the torsional motions under the trimer intermolecular potential.

In Refs. [15,17], the effective Hamiltonians are derived from Eq. (2) for all torsional states $|k, n\rangle$ of trimers. For non-degenerate states $|k, n\rangle$ with $k = 0$ or 3 (modulo 6), the effective Hamiltonian is

$$H^{\text{rot}}_{\text{eff}}(k, n) = B^{(k,n)}(J_x^2 + J_y^2) + C^{(k,n)}J_z^2, \tag{3}$$

while for states $|k, n\rangle$ with $k = \pm 1$ or ± 2 (modulo 6), the effective rotational Hamiltonian becomes

$$\begin{aligned} H^{\text{rot}}_{\text{eff}}(k, k', n) = {} & \delta_{k',k}[B^{(|k|,n)}(J_x^2 + J_y^2) + C^{(|k|,n)}J_z^2] \\ & \pm \delta_{k',k}(-2\zeta_{k',k}C^{(|k|,n)})J_z \\ & + \delta_{k',k-2\ (\text{modulo } 6)}\mu_{--}^{(|k|,n)}J_-J_- \\ & + \delta_{k',k+2\ (\text{modulo } 6)}\mu_{++}^{(|k|,n)}J_+J_+, \end{aligned} \tag{4}$$

with $\mu_{--}^{(1,n)} = [\mu_{++}^{(-1,n)}]^*$ and $\mu_{--}^{(-2,n)} = [\mu_{++}^{(+2,n)}]^*$. The definitions of $\mu_{--}^{(|k|,n)}$ and $\mu_{++}^{(|k|,n)}$ can be found in Ref. [15], where $\mu_{--}^{(|k|,n)}$ and $\mu_{++}^{(|k|,n)}$ represent the second-order Coriolis couplings. In the first-order Coriolis term, the plus sign is for $k = +1$ or $k = -2$, and the minus sign is for $k = -1$ or $k = +2$.

3. Experiment

The Berkeley terahertz spectrometer used in the observation of the new region around 2.9 THz has been described previously [30,31], and only brief features and improvements relevant to this experiment will be given here. Tunable terahertz laser radiation is generated by nonlinear mixing of fixed-frequency THz radiation with tunable micro- or millimeter-wave radiation in a Schottky barrier diode. This tunable THz laser beam possesses the

sum and difference frequencies of the given THz laser (ν_0) and the microwave (ν_m), viz. $\nu = \nu_0 \pm \nu_m$. The fundamental, first, or second harmonic of a HP8367B microwave synthesizer (2–26 GHz) and two millimeter wave synthesizers (53–78 and 78–118 GHz, Kvarz, Russia) are employed to provide a continuously variable frequency scan from 2 to 118 GHz around a given THz laser line. In this Letter, the 9P(22) transition of a line tunable high power CO_2 laser is used to pump the THz laser line of the frequency 2.89970824 THz (103.5 μm, $^{13}CH_3OH$) and the CO_2 transition 9R(10) is used to pump 3.1059368 THz (96.5 μm, CH_3OH) laser line for the continuous scan from 2.779 to 3.047 THz.

The D_2O water clusters, $(D_2O)_n$, are produced by the supersonic expansion from a slit of 101.6 mm length and 100 μm width. The argon carrier gas is passed through a D_2O water container and the D_2O saturated mixture is then expanded through the slit to the vacuum chamber, which is pumped by a Roots blower (Edwards EH4200) backed by two rotary pumps. The gas pulse is gated at 45 Hz with an average backing pressure around 450 Torr. The THz beams cross the expanded gas 22 times in an optical Herriott cell. Frequency modulation (29 kHz) and 2f lock-in methods are used, and 25 signals are averaged for each laser frequency with a scanning step size of 200 kHz.

4. Analysis and results

As mentioned in the previous section, the water trimer VRT spectra have characteristic quartet splittings, and for $(D_2O)_3$, this quartet splitting is just a few MHz. This feature makes the D_2O trimer spectrum easily identifiable. A typical D_2O trimer transition is shown in Fig. 3a, with nuclear spin statistical weights near (76:108:54:11) for the quartet splitting peaks and a splitting of around 5 MHz. Except for very strong transitions, usually only the three strongest absorption peaks are observable. The irregular intensity pattern with nuclear spin statistical weights of roughly (245:50:108:75) only occurs in the transitions with $K = 0 \leftarrow 1$, as shown in Fig. 3b.

Fig. 4 shows the D_2O trimer stick spectrum in the region from 2779 to 3047 GHz. A total of 218 transitions, including 149 new transitions, were observed and are listed in Table 1, with the best signal-to-noise ratio being about 80. There, each stick transition actually represents three or four absorption peaks. The transition frequencies listed in Table 1 correspond only to the strongest absorption peak except for the irregular intensity pattern with $K = 0 \leftarrow 1$ transitions. The first fit was performed by excluding transitions with the irregular intensity patterns, and then the obtained fitting parameters were used to predict those transitions. The predicted frequencies were found to be closest to the second strongest peaks; therefore, we chose the second strong peaks to represent the $K = 0 \leftarrow 1$ series transitions in the final fitting. The transition frequencies are listed in Table 1. In Fig. 4, a spectral feature is clearly evident in the strong R branch region; the D_2O trimer transitions display a parallel band-like pattern with a spacing of around 6 GHz, approximately one B (rather than two B) value of the D_2O trimer. Similar 6 GHz spacings are shown in the Q branch region as well, displayed in Fig. 4. These features indicate a planar structure for the D_2O trimer, with the transitions obeying perpendicular selection rules.

The rotational assignment of the transitions is quite straightforward. Sixty-nine transitions located in the region from 2883 to 2962 GHz had been observed, assigned, and well-fitted before [12,15]. These include most of the Q branch transitions with $K' = 0$–5 and $J' = 0$–8, and some P branch transitions with $J' = 0$–6 and $K' = 0$–6. This region has now been rescanned, and only a few new

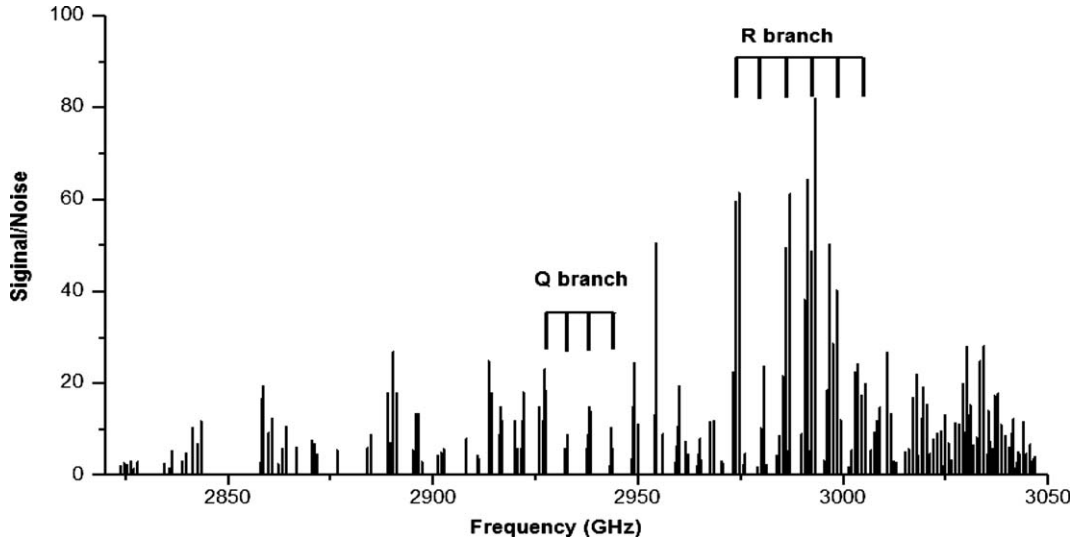

Fig. 4. The stick spectrum of the $(D_2O)_3 \pm 2^1 \leftarrow 0^0$ torsional perpendicular band. Spacings of B (about 6 GHz) are seen in both the R and Q branches, and indicate a planar average structure for the water trimer.

Table 1
Observed VRT transitions (MHz) of the $\pm 2^1 \leftarrow 0^0$ $(D_2O)_3$ torsional band

$J'_{K'} \leftarrow J''_{K''}$	Frequency/MHz	Residual	$J'_{K'} \leftarrow J''_{K''}$	Frequency/MHz	Residual
	$+2^1 \leftarrow 0^0$			$-2^1 \leftarrow 0^0$	
$13_8 \leftarrow 14_9$	2823772.4	−3.6	$8_2 \leftarrow 9_1$	2827894.7	1.9
$12_6 \leftarrow 13_7$	2824467.2	0.6	$7_3 \leftarrow 8_2$	2834264.0	0.1
$11_4 \leftarrow 12_5$	2825223.3	−1.1	$7_2 \leftarrow 8_1$	2839622.0	2
$10_2 \leftarrow 11_3$	2826051.9	−0.1	$5_3 \leftarrow 6_2$	2857668.5	−1.8
$9_0 \leftarrow 10_1$	2826953.5	0.5	$5_2 \leftarrow 6_1$	2863031.3	1.5
$12_8 \leftarrow 13_9$	2835563.0	−1.7	$1_1 \leftarrow 1_0$	2938213.0	−1.5
$11_6 \leftarrow 12_7$	2836243.8	−0.2	$2_1 \leftarrow 2_0$	2938158.0	−2.1
$8_0 \leftarrow 9_1$	2838685.3	−1.4	$3_1 \leftarrow 3_0$	2938077.0	−1.6
$12_9 \leftarrow 13_{10}$	2841138.7	−3.8	$4_1 \leftarrow 4_0$	2937968.0	−2
$10_5 \leftarrow 11_6$	2842493.0	2.9	$5_1 \leftarrow 5_0$	2937833.0	−1.2
$9_3 \leftarrow 10_4$	2843262.9	1	$6_1 \leftarrow 6_0$	2937671.0	−0.4
$12_{12} \leftarrow 13_{13}$	2857976.0	−0.8	$7_1 \leftarrow 7_0$	2937483.0	1.4
$11_{10} \leftarrow 12_{11}$	2858521.4	0.1	$8_1 \leftarrow 8_0$	2937268.0	3.2
$9_6 \leftarrow 10_7$	2859772.8	2.9	$2_2 \leftarrow 2_1$	2932801.0	1.7
$8_4 \leftarrow 9_5$	2860488.1	1.9	$3_2 \leftarrow 3_1$	2932741.0	1.2
$6_0 \leftarrow 7_1$	2862122.2	3.2	$4_2 \leftarrow 4_1$	2932662.0	1.6
$11_{11} \leftarrow 12_{12}$	2864134.6	0.2	$5_2 \leftarrow 5_1$	2932562.0	1
$7_3 \leftarrow 8_4$	2866729.5	−2.3	$6_2 \leftarrow 6_1$	2932443.0	1.6
$10_{10} \leftarrow 11_{11}$	2870297.1	1.8	$7_2 \leftarrow 7_1$	2932304.0	2.3
$9_8 \leftarrow 10_9$	2870878.8	1.5	$3_3 \leftarrow 3_2$	2927375.6	−3.9
$8_6 \leftarrow 9_7$	2871518.0	2.1	$4_3 \leftarrow 4_2$	2927296.5	−4.5
$9_9 \leftarrow 10_{10}$	2876453.8	−5.5	$5_3 \leftarrow 5_2$	2927198.7	−4.2
$6_4 \leftarrow 7_5$	2883934.0	0.8	$6_3 \leftarrow 6_2$	2927079.3	−5.7
$5_2 \leftarrow 6_3$	2884683.0	1.3	$7_3 \leftarrow 7_2$	2926948.0	0.5
$7_7 \leftarrow 8_8$	2888796.0	−0.2	$8_3 \leftarrow 8_2$	2926792.0	1.8
$6_5 \leftarrow 7_6$	2889440.3	−0.3	$4_4 \leftarrow 4_3$	2921963.0	0.7
$5_3 \leftarrow 6_4$	2890147.0	−0.6	$5_4 \leftarrow 5_3$	2921866.0	0.7
$4_1 \leftarrow 5_2$	2890920.0	−0.2	$6_4 \leftarrow 6_3$	2921749.0	0.1
$6_6 \leftarrow 7_7$	2894969.0	0.3	$7_4 \leftarrow 7_3$	2921613.0	−0.1
$5_4 \leftarrow 6_5$	2895635.0	−0.1	$8_4 \leftarrow 8_3$	2921458.0	0.1
$4_2 \leftarrow 5_3$	2896366.0	0.4	$9_4 \leftarrow 9_3$	2921284.0	0.7
$3_0 \leftarrow 4_1$	2897162.5	0.4	$5_5 \leftarrow 5_4$	2916551.0	3.1
$5_5 \leftarrow 6_6$	2901145.9	2.1	$6_5 \leftarrow 6_4$	2916434.0	1
$4_3 \leftarrow 5_4$	2901833.6	0.9	$7_5 \leftarrow 7_4$	2916299.0	0.1
$3_1 \leftarrow 4_2$	2902587.1	0.4	$8_5 \leftarrow 8_4$	2916146.0	0.3
$3_2 \leftarrow 4_3$	2908033.1	0	$7_6 \leftarrow 7_5$	2911005.9	1.6
$3_3 \leftarrow 4_4$	2913501.0	−0.2	$8_6 \leftarrow 8_5$	2910854.4	1.2
$2_1 \leftarrow 3_2$	2914237.0	0.9	$1_1 \leftarrow 0_0$	2949822.9	1.4
$2_2 \leftarrow 3_3$	2919683.0	−0.3	$2_2 \leftarrow 1_1$	2955983.0	−1
$1_0 \leftarrow 2_1$	2920444.7	3.2	$2_1 \leftarrow 1_0$	2961385.0	−2.8
$1_1 \leftarrow 2_2$	2925866.0	−1.4	$3_3 \leftarrow 2_2$	2962154.7	−0.7
$0_0 \leftarrow 1_1$	2932053.9	0.3	$3_2 \leftarrow 2_1$	2967514.8	−0.2
$11_{10} \leftarrow 11_{11}$	2997548.1	1.4	$4_4 \leftarrow 3_3$	2968329.1	0.7
$10_9 \leftarrow 10_{10}$	2992149.3	0.9	$3_1 \leftarrow 2_0$	2972941.9	2
$11_9 \leftarrow 11_{10}$	2991931.6	2.1	$4_3 \leftarrow 3_2$	2973665.7	0.2
$12_9 \leftarrow 12_{10}$	2991694.5	1.7	$5_5 \leftarrow 4_4$	2974505.6	2.5
$13_9 \leftarrow 13_{10}$	2991437.5	−1.1	$4_2 \leftarrow 3_1$	2979024.7	0.7
$9_8 \leftarrow 9_9$	2986749.4	−2.2	$5_4 \leftarrow 4_3$	2979818.8	1.1
$10_8 \leftarrow 10_9$	2986553.7	2.8	$6_6 \leftarrow 5_5$	2980681.1	1.6
$11_8 \leftarrow 11_9$	2986334.7	2.8	$4_1 \leftarrow 3_0$	2984478.2	1
$12_8 \leftarrow 12_9$	2986097.6	2.6	$5_3 \leftarrow 4_2$	2985155.0	1.8
$8_7 \leftarrow 8_8$	2981357.1	1	$6_5 \leftarrow 5_4$	2985973.5	2.1
$9_7 \leftarrow 9_8$	2981178.1	3.8	$7_7 \leftarrow 6_6$	2986861.6	4.2
$7_6 \leftarrow 7_7$	2975962.9	0.9	$5_2 \leftarrow 4_1$	2990511.4	1.3
$8_6 \leftarrow 8_7$	2975801.9	2.2	$6_4 \leftarrow 5_3$	2991283.6	−0.4
$9_6 \leftarrow 9_7$	2975620.4	2.2	$7_6 \leftarrow 6_5$	2992128.6	1.7
$6_5 \leftarrow 6_6$	2970565.4	−3.9	$8_8 \leftarrow 7_7$	2993039.9	2.9
$7_5 \leftarrow 7_6$	2970424.0	−2.8	$5_1 \leftarrow 4_0$	2995999.2	0.3
$8_5 \leftarrow 8_6$	2970267.5	2.6	$6_3 \leftarrow 5_2$	2996618.2	0.6
$5_4 \leftarrow 5_5$	2965179.0	1.1	$7_5 \leftarrow 6_4$	2997417.6	1.3
$6_4 \leftarrow 6_5$	2965057.4	1.7	$8_7 \leftarrow 7_6$	2998286.0	2
$7_4 \leftarrow 7_5$	2964915.1	1.4	$9_9 \leftarrow 8_8$	2999221.5	3.4
$8_4 \leftarrow 8_5$	2964755.6	3.1	$6_2 \leftarrow 5_1$	3001974.9	2.3

Table 1 (*continued*)

$J'_{K'} \leftarrow J''_{K''}$	Frequency/MHz	Residual	$J'_{K'} \leftarrow J''_{K''}$	Frequency/MHz	Residual
$9_4 \leftarrow 9_5$	2964574.4	2.2	$7_4 \leftarrow 6_3$	3002727.5	0.9
$10_4 \leftarrow 10_5$	2964372.1	−1.3	$8_6 \leftarrow 7_5$	3003551.8	1.4
$4_3 \leftarrow 4_4$	2959789.0	1.1	$9_8 \leftarrow 8_7$	3004445.6	2.8
$5_3 \leftarrow 5_4$	2959688.0	1.9	$10_{10} \leftarrow 9_9$	3005404.6	3.8
$6_3 \leftarrow 6_4$	2959566.0	1.6	$6_1 \leftarrow 5_0$	3007506.2	1.8
$7_3 \leftarrow 7_4$	2959426.3	3.1	$7_3 \leftarrow 6_2$	3008059.7	1.6
$8_3 \leftarrow 8_4$	2959266.9	4.1	$8_5 \leftarrow 7_4$	3008839.4	2.3
$9_3 \leftarrow 9_4$	2959086.3	2.8	$10_9 \leftarrow 9_8$	3010605.8	2.3
$3_2 \leftarrow 3_3$	2954399.0	−0.3	$11_{11} \leftarrow 10_{10}$	3011588.2	3.3
$4_2 \leftarrow 4_3$	2954317.9	−0.1	$9_6 \leftarrow 8_5$	3014949.4	−0.1
$5_2 \leftarrow 5_3$	2954217.6	0.8	$10_8 \leftarrow 9_7$	3015822.2	−1.9
$6_2 \leftarrow 6_3$	2954097.2	1.3	$11_{10} \leftarrow 10_9$	3016763.3	−2.5
$2_1 \leftarrow 2_2$	2949012.9	0.9	$12_{12} \leftarrow 11_{11}$	3017768.9	−1.7
$3_1 \leftarrow 3_2$	2948952.7	1.4	$7_1 \leftarrow 6_0$	3018991.6	−1.4
$4_1 \leftarrow 4_2$	2948872.6	2	$8_3 \leftarrow 7_2$	3019471.8	−2
$5_1 \leftarrow 5_2$	2948770.9	0.8	$9_5 \leftarrow 8_4$	3020231.0	−2.1
$6_1 \leftarrow 6_2$	2948651.4	1.2	$10_7 \leftarrow 9_6$	3021061.4	−2.4
$7_1 \leftarrow 7_2$	2948512.3	1.2	$11_9 \leftarrow 10_8$	3021961.9	−2
$8_1 \leftarrow 8_2$	2948355.3	2	$12_{11} \leftarrow 11_{10}$	3022928.8	−1.2
$1_0 \leftarrow 1_1$	2943626.5	0.4	$13_{13} \leftarrow 12_{12}$	3023955.7	−1.9
$2_0 \leftarrow 2_1$	2943586.3	0.4	$8_2 \leftarrow 7_1$	3024823.0	−0.2
$3_0 \leftarrow 3_1$	2943525.9	0.2	$9_4 \leftarrow 8_3$	3025536.1	−1.8
$4_0 \leftarrow 4_1$	2943444.9	−0.9	$10_6 \leftarrow 9_5$	3026321.5	−1.9
$5_0 \leftarrow 5_1$	2943345.3	−0.1	$11_8 \leftarrow 10_7$	3027177.2	−2.9
$6_0 \leftarrow 6_1$	2943226.0	0.1	$12_{10} \leftarrow 11_9$	3028104.5	−1.1
$7_0 \leftarrow 7_1$	2943083.4	−3.8	$13_{12} \leftarrow 12_{11}$	3029095.5	−0.5
$3_1 \leftarrow 2_2$	2983727.8	0.6	$14_{14} \leftarrow 13_{13}$	3030144.0	−2.1
$4_0 \leftarrow 3_1$	2989809.4	0	$8_1 \leftarrow 7_0$	3030463.7	−0.5
$4_1 \leftarrow 3_2$	2995235.4	0.3	$9_3 \leftarrow 8_2$	3030862.2	−1.8
$5_0 \leftarrow 4_1$	3001297.1	1.5	$10_5 \leftarrow 9_4$	3031601.1	−2.6
$5_1 \leftarrow 4_2$	3006721.5	1	$11_7 \leftarrow 10_6$	3032413.9	−1.8
$5_2 \leftarrow 4_3$	3012169.5	0.4	$12_9 \leftarrow 11_8$	3033296.6	−2.1
$6_0 \leftarrow 5_1$	3012757.9	−1.2	$13_{11} \leftarrow 12_{10}$	3034249.2	−0.3
$6_1 \leftarrow 5_2$	3018177.9	−4.9	$14_{13} \leftarrow 13_{12}$	3035265.7	2
$7_0 \leftarrow 6_1$	3024195.1	−4.6	$15_{15} \leftarrow 14_{14}$	3036334.0	−1.9
$7_1 \leftarrow 6_2$	3029617.0	−4.7	$9_2 \leftarrow 8_1$	3036209.8	0.1
$7_2 \leftarrow 6_3$	3035066.9	−2.1	$10_4 \leftarrow 9_3$	3036903.8	−1.4
$8_0 \leftarrow 7_1$	3035616.7	−0.4	$11_6 \leftarrow 10_5$	3037669.9	−1.5
$7_3 \leftarrow 6_4$	3040538.6	−2	$12_8 \leftarrow 11_7$	3038509.7	−0.6
$8_1 \leftarrow 7_2$	3041032.6	−4.3	$13_{10} \leftarrow 12_9$	3039419.9	0.4
$7_4 \leftarrow 6_5$	3046034.0	−2.3	$14_{12} \leftarrow 13_{11}$	3040398.4	2.9
$8_2 \leftarrow 7_3$	3046480.7	−2.4	$15_{14} \leftarrow 14_{13}$	3041435.3	2
			$16_{16} \leftarrow 15_{15}$	3042525.4	−1.6
			$9_1 \leftarrow 8_0$	3041918.1	1
			$10_3 \leftarrow 9_2$	3042229.7	1.7
			$11_5 \leftarrow 10_4$	3042948.0	0
			$12_7 \leftarrow 11_6$	3043741.3	−0.1
			$13_9 \leftarrow 12_8$	3044607.3	0.1
			$14_{11} \leftarrow 13_{10}$	3045545.9	3.2
			$15_{13} \leftarrow 14_{12}$	3046550.3	6.7

Residuals are from the global fit including all 823 transitions involving six observed torsional bands. Each frequency represents three or four absorption peaks split by bifurcation tunneling. For $K = 0 \leftarrow 1$ transitions, the frequencies listed here correspond to the second strongest peaks; all other frequencies correspond to the strongest peaks of the bifurcation multiplets.

transitions have been observed. The new spectral search completed the whole P, Q and R branch regions. The predictions of new transitions based on the previous fitting parameters are in reasonable agreement with the newly observed 149 transitions. As listed in Table 1, the assignment for the complete band makes the upper states (J', K') up to (12, 12) for the sub-band $+2^1 \leftarrow 0^0$ and (16, 16) for the sub-band $-2^1 \leftarrow 0^0$. The highest J' and K' values occur in the P branch for the sub-band $+2^1 \leftarrow 0^0$ with the rule $K' - K'' = -1$, while they occur in the R branch for the sub-band $-2^1 \leftarrow 0^0$ with the rule $K' - K'' = +1$.

A global fit has been made for all observed rovibrational transitions of the torsional bands shown in Fig. 1. The Hamiltonians employed are given in Eqs. (3) and (4) for the non-degenerate and degenerate states, respectively. A total of 823 transitions were fitted in the new global analysis, including the 149 newly observed transitions of the band $\pm 2^1 \leftarrow 0^0$. A total of 50 parameters were varied in

Table 2
The D_2O trimer molecular constants for the torsional states derived from the global fit of 823 transitions in six observed torsional bands

k^n	0^0	$+1^0$	-1^0	$+2^0$	-2^0	3^0	3^1	$+2^1$	-2^1
E_0	0.0[a]	255977.3(4)		839187.2(4)		1232139.3(5)	2709548.8(6)	2940937.6(3)	
$B(=A)$	5796.35(2)	5795.97(2)		5794.66(3)		5792.89(4)	5788.68(3)	5786.32(2)	
C	3087.71(1)	3090.47(2)		3095.82(2)		3099.55(3)	3089.84(3)	3088.61(1)	
D_J	0.0296(2)	0.0282(2)	0.0278(2)	0.0276(3)	0.0273(3)	0.0268(6)	0.0274(4)	0.0279(3)	0.0292(3)
D_{JK}	−0.0405(5)	−0.0469(6)	−0.0459(6)	−0.0430(7)	−0.0421(8)	−0.043(1)	−0.0397(9)	−0.0460(7)	−0.0438(6)
D_K	0.0121(8)	0.0198(7)	0.0188(9)	0.0173(8)	0.015(1)	0.017(1)	0.0129(9)	0.019(1)	0.0158(8)
ζ	–	−0.04388(1)		−0.04822(1)		–	–	0.00029(1)	
$\lvert\mu_{++}\rvert$	–	26.68(1)		13.73(2)		–	–	3.599(9)	

The parameters A, B, C, D_J, D_{JK}, and D_K are the usual symmetric top rotational and distortion constants in units of MHz. The ζ (dimensionless) and μ_{++} are the Coriolis coupling constants. 1σ uncertainties of fitted parameters are given in parentheses, corresponding to a 1.73 MHz standard deviation of the global fit.

[a] Fixed in the fitting.

the global fit, and the improved molecular constants of the D_2O trimer are presented in Table 2 for the observed torsional states. The standard deviation of 1.73 MHz is less than the experimental uncertainty of 2 MHz.

5. Conclusion and discussion

The highest energy torsional band yet observed ($\pm 2^1 \leftarrow 0^0$), encompassing a total of 218 transitions, has been observed and assigned in accord with perpendicular selection rules. The planar vibrationally averaged water trimer structure is evidenced in the newly observed R and Q branches. A global analysis including all of the observed torsional rovibrational transitions yields improved molecular constants describing the torsional motions.

This band provides a good test of the Hamiltonians developed for the torsional vibrations of the water trimer [15,26], because transitions with very high $J' = 16$ and $K' = 16$ values have been observed, and no significant perturbations have been found in the spectra. We intentionally made these high J and K transitions observable by reducing the backing pressure, which increases the rotational temperature (to around 10 K) in the supersonic expansions. The fitting results confirm the validity of the developed model, although the residuals are somewhat larger for some transitions with high values of J and K. Higher-order distortion constants may be needed in the fit if still higher J and K transitions are observed for the bands.

We note that the power of the terahertz sideband beam varies considerably from one spectral region to another. The transition intensities from such different regions are thus not meaningful, but in a short scan region and time, the relative intensities faithfully represent the nuclear spin weight for the transitions. As shown in Fig. 3, the 5 MHz quartet splitting and the (76:108:54:11) nuclear spin weights have been observed for all transitions except for the transitions in $K = 0 \leftarrow 1$ series. The irregular intensity pattern for $K = 0 \leftarrow 1$ series has been observed in all those torsional bands from the ground state, $\pm 2^0 \leftarrow 0^0$ and $\pm 2^1 \leftarrow 0^0$. This irregular pattern of the bifurcation tunneling splitting has been addressed in detail in Refs. [27–29], and the overall spin weight ratio is predicted to be 248:54:108:70 for the band $\pm 2^1 \leftarrow 0^0$, which matches well with our observed (35:10:15:12) value.

The torsional vibration energy levels of water trimers were previously calculated [32,33] and helped to unambiguously assign the observed torsional bands [15,17], including this, the highest measured torsional band. The calculations are based on the three-dimensional (the out of plane bending angles) torsional potentials, and the ab initio potential energy surfaces of the water trimer torsional motions were derived by Burgi, Graf, Leutwyler, and Klopper (BGLK potential) [34], and by van Duijneveldt-van de Rijdt and van Duijneveldt (DD potential) [35]. In Table 3, the calculated torsional energy levels (under 150 cm^{-1}) and experimental results are listed for the D_2O trimer. The calculation [32] based on the DD potential is closer to experimental data for the lowest three levels, and the calculations [32,33] based on BGLK and the coupled three-dimensional (3D) potentials better match experiments for higher torsional energy levels. This indicates that next two highest torsional vibrational levels should be found around 117 and 130 cm^{-1} for the D_2O trimer.

Table 3
The calculated and experimental energy levels of $(D_2O)_3$ torsional vibrations (cm^{-1})

$\lvert k^n\rangle$	DD[a]	BGLK[a]	3D[b]	Experimental
0^0	0.0	0.0	0.0	0.0
$\pm 1^0$	7.68	5.15	4.966	8.53848
$\pm 2^0$	25.18	17.15	16.597	27.99227
3^0	36.61	24.73	23.970	41.09974
3^1	96.14	88.92	87.438	90.38082
$\pm 2^1$	107.50	98.26	96.914	98.09912
$\pm 1^1$	129.74	117.76	116.566	–
0^1	132.47	130.06	129.020	–
0^2	143.22	151.60	151.367	–

The experimental data are from the current global fit.

[a] Ref. [32] based on the DD and BGLK potentials, respectively.

[b] Ref. [33] based on the coupled 3D potential.

Acknowledgements

This work was supported by the Experimental Physical Chemistry Division of the National Science Foundation.

We warmly thank Dr. Mac G. Brown for his considerable help in using the fitting program.

References

[1] K. Liu, J.D. Cruzan, R.J. Saykally, Science 271 (1996) 929.
[2] F.N. Keutsch, R.J. Saykally, PNAS 98 (2001) 10533.
[3] C.J. Burnham, S.S. Xantheas, J. Chem. Phys. 116 (2002) 5115.
[4] R.S. Fellers, C. Leforestier, L.B. Braly, M.G. Brown, R.J. Saykally, Science 284 (1999) 945.
[5] N. Goldman, R.S. Fellers, M.G. Brown, L.B. Braly, C.J. Keoshian, C. Leforestier, R.J. Saykally, J. Chem. Phys. 116 (2002) 10148.
[6] C. Leforestier, F. Gatti, R.S. Fellers, R.J. Saykally, J. Chem. Phys. 117 (2002) 8710.
[7] N. Goldman, R.J. Saykally, J. Chem. Phys. 120 (2004) 4777.
[8] L. Ojamae, K. Hermansson, J. Phys. Chem. 98 (1994) 4271.
[9] M.P. Hodges, A.J. Stone, S.S. Xantheas, J. Phys. Chem. A 101 (1997) 9163.
[10] E.M. Mas, R. Bukowski, K. Szalewicz, J. Chem. Phys. 118 (2003) 4386.
[11] N. Pugliano, R.J. Saykally, Science 257 (1992) 1937.
[12] K. Liu, J.G. Loeser, M.J. Elrod, B.C. Host, J.A. Rzepiela, N. Pugliano, R.J. Saykally, J. Am. Chem. Soc. 116 (1994) 3507.
[13] K. Liu, M.J. Elrod, J.G. Loeser, J.D. Cruzan, N. Pugliano, M.G. Brown, J. Rzepiela, R.J. Saykally, Faraday Discuss. 35 (1994) 34.
[14] S. Suzuki, G.A. Blake, Chem. Phys. Lett. 229 (1994) 499.
[15] M.R. Viant, M.G. Brown, J.D. Cruzan, R.J. Saykally, M. Geleijns, A. van der Avoird, J. Chem. Phys. 110 (1999) 4369.
[16] F.N. Keutsch, E.N. Karyakin, R.J. Saykally, A. van der Avoird, J. Chem. Phys. 114 (2001) 3988.
[17] M.G. Brown, M.R. Viant, R.P. McLaughlin, C.J. Keoshian, E. Michael, J.D. Cruzan, R.J. Saykally, A. van der Avoird, J. Chem. Phys. 111 (1999) 7789.
[18] K. Liu, M.G. Brown, M.R. Viant, J.D. Cruzan, R.J. Saykally, Mol. Phys. 89 (1996) 1373.
[19] M.R. Viant, J.D. Cruzan, D.D. Lucas, M.G. Brown, K. Liu, R.J. Saykally, J. Phys. Chem. A 101 (1997) 9032.
[20] F.N. Keutsch, M.G. Brown, P.B. Petersen, R.J. Saykally, M. Geleijns, A. van der Avorid, J. Chem. Phys. 114 (2001) 3994.
[21] F.N. Keutsch, R.S. Fellers, M.R. Viant, R.J. Saykally, J. Chem. Phys. 114 (2001) 4005.
[22] F.N. Keutsch, J.D. Cruzan, R.J. Saykally, Chem. Rev. 103 (2003) 2533.
[23] J.E. Fowler, H.F. Schaefer, J. Am. Chem. Soc. 117 (1995) 446.
[24] D.J. Wales, J. Am. Chem. Soc. 115 (1993) 11180.
[25] S.S. Xantheas, T.H. Dunning Jr., J. Chem. Phys. 99 (1993) 8774.
[26] A. van der Avoird, E.H.T. Olthof, P.E.S. Wormer, J. Chem. Phys. 105 (1996) 8034.
[27] E.H.T. Olthof, A. van der Avoird, P.E.S. Wormer, K. Liu, R.J. Saykally, J. Chem. Phys. 105 (1996) 8051.
[28] F.K. Keutsch, R.J. Saykally, D.J. Wales, J. Chem. Phys. 117 (2002) 8823.
[29] M. Takahashi, Y. Watanabe, T. Taketsugu, D.J. Wales, J. Chem. Phys. 123 (2005) 044302.
[30] G.A. Blake, K.B. Laughlin, R.C. Cohen, K.L. Busarow, D.H. Gwo, C.A. Schmuttenmaer, D.W. Steyert, R.J. Saykally, Rev. Sci. Instrum. 62 (1991) 1701.
[31] K. Liu, R.S. Fellers, M.R. Viant, R.P. McLaughlin, M.G. Brown, R.J. Saykally, Rev. Sci. Instrum. 67 (1996) 410.
[32] M. Geleijns, A. van der Avoird, J. Chem. Phys. 110 (1999) 823.
[33] D. Sabo, Z. Bacic, T. Burgi, S. Leutwyler, Chem. Phys. Lett. 244 (1995) 283.
[34] T. Burgi, S. Graf, S. Leutwyler, W. Klopper, J. Chem. Phys. 103 (1995) 1077.
[35] J.G.C.M. van Duijneveldt-van de Rijdt, F.B. van Duijneveldt, Chem. Phys. Lett. 237 (1995) 560.